Theoretical Study of Stratospheric Relevant Anions: Nitrate−Nitric Acid Complexes

O. Gálvez*,† and P. C. Gómez‡

Departamento Química Física I. Facultad de C.C. Químicas, Universidad Complutense de Madrid, 28040 Madrid, Spain

Luis F. Pacios§

Unidad de Química y Bioquímica, Departamento de Biotecnología, E.T.S.I. Montes, Universidad Politécnica de Madrid, 28040 Madrid, Spain

Received: October 17, 2005; In Final Form: January 18, 2006

The ion complexes $NO_3^-(HNO_3)_n$, $n = 1-3$, have been studied by means of ab initio calculations at the B3LYP/aug-cc-pVTZ level of theory. These systems are the most abundant anionic clusters below approximately 30 km altitude in the stratosphere and also in the upper troposphere. These complexes display short strong hydrogen bonds, which should be considered to explain their abundance in the atmosphere. Equilibrium geometries, harmonic frequencies, relative energies, and thermochemical data have been calculated for these anions for the first time. The calculations indicate small differences of energy in the variation of the two nitrate groups from planarity to an almost perpendicular form for $n = 1$. Planar geometries are found for $n = 2$ and 3 to give rise to a highly symmetric C_{3h} $NO_3^-(HNO_3)_3$. In all the cases, binding energies close to those of covalent compounds are estimated. When experimental data are available, good correlations are found with our results.

I. Introduction

Because electrical conductivity of the atmospheric medium is directly influenced by the chemical nature of ions in the atmosphere, stratospheric ions are of considerable interest. Also, they may influence stratospheric trace gases (via ion−molecule or ion-catalyzed reactions[1]), and formation of aerosols (via ion-induced nucleation[2]). To know the ion composition in the stratosphere, efforts were undertaken in the mid 1970s and 1980s to develop balloon-borne ion mass spectrometers. Several in situ stratospheric ion composition measurements were performed in the altitude region from 15 to 45 km, mainly by two groups: the Max-Planck-Institut für Kernphysik in Heidelberg (MPIH) and the Belgian Institute for Space Aeronomy (BISA) (ref 3 and references therein). Under normal conditions, the principal ionization source in the stratosphere is galactic cosmic rays. In the lower stratosphere, cosmic rays generate ions at a rate of about 10 ion pairs/(cm^3·s), which is nearly constant in time and space.[4] The positive species generated include hydronium ions of the type $H^+(H_2O)_n$, also called proton hydrates (PHs) and a second group of ions, called nonproton hydrates (NPHs) with a general formula $H^+(CH_3CN)_m(H_2O)_n$.[5] PHs are dominant at higher altitudes than NPHs. For the negative ions, mechanisms of productions are reported elsewhere,[6] so that we will outline here just the most important processes. The first negative ion in the stratosphere is produced by the attachment of free electrons to oxygen molecules resulting in the primary O_2^-, which is converted quickly into CO_3^- and CO_4^- by reaction with relatively abundant trace gases as CO_2. These ions react with nitrogen oxides (such as NO and NO_2) to form NO_3^-, which is very stable due to its electronic configuration. NO_3^- reacts with relatively abundant water vapor resulting in $NO_3^-(H_2O)_n$ type ions. However, this process does not play a major role because $NO_3^-(H_2O)_n$ are weakly bound ions. As a result, nitric and sulfuric acid replace H_2O, both reactions competing each other.[7] Following this scheme, the two main negative ions families in the stratosphere are formed by the terminal nitrate and bisulfate clusters, denoted as $NO_3^-(HNO_3)_m(H_2SO_4)_n$ and $HSO_4^-(H_2SO_4)_m(HNO_3)_n$. Bisulfate ion is produced by a fast switching reaction between the nitrate ion and sulfuric acid vapor. Below approximately 30 km, NO_3^- core ions are dominant, but HSO_4^- core ions are more abundant above this height.[8,9] Also, a reverse changeover with NO_3^- core ions becoming again dominant at 42 km is predicted by models[10] and confirmed by measurements in the upper stratosphere.[11] The negative ion $NO_3^-(HNO_3)_2$ dominates at heights between 15 and 32 km, and in the middle height region around 27−30 km, accounting for over 90% of all negative ions detected.[8] These observations were done at mid-latitudes but similar results were obtained at the Arctic vortex, where ions containing NO_3^- cores account for more than 95% of all ions detected between 24 and 30 km.[12] But the importance of NO_3^- core ions lies not only in the stratosphere. Recent models suggest that the dominant negative ions in the troposphere, for nighttime conditions, are of the type $NO_3^-HNO_3H_2O$ and $NO_3^-(HNO_3)_n$[13] in good agreement with the measurements reported.[14]

Contrary to the positive ions, which have received great attention (see for example ref 15 and references therein), few studies have been carried out to elucidate the structures and properties of negative ions. Despite the significance of the $NO_3^-(HNO_3)_n$ ions, only the structure of $NO_3^-HNO_3$ has been reported in the literature from X-ray and neutron diffraction data,[16,17] infrared and Raman spectroscopy[18] (always in solid phase) and ab initio calculations at low levels of theory.[19−21]

* Corresponding author.
† E-mail: ogalvez@quim.ucm.es.
‡ E-mail: pgomez@quim.ucm.es.
§ E-mail: luis.fpacios@upm.es.

10.1021/jp055935m CCC: $33.50
Published on Web 02/16/2006

The properties of $NO_3^-(HNO_3)_n$ ions are characterized by the features of their short strong hydrogen bonds (SSHBs). The use of ab initio methodology to study issues related with SSHBs has become nearly a routine tool.[22−25] However, to directly address the geometries and energetics of these systems, one must resort to high-level ab initio calculations including electron correlation and flexible basis sets. In this work, we apply such an approach to the $NO_3^-(HNO_3)_n$ family of ions for the first time. The quantum methodology employed is addressed in the next section, and then our results are reported and discussed. Finally, a brief section summarizes our main conclusions.

II. Calculations

Quantum calculations were performed with the hybrid DFT method B3LYP, which consists of a mixture of Hartree−Fock (HF) exchange with Becke's three parameters exchange functional plus the nonlocal correlation functional of Lee, Yang, and Parr. Furthermore, MP2 and CCSD(T) methods were also used in some systems to contrast with B3LYP calculations. Because the size n of $NO_3^-(HNO_3)_n$ cluster increases from 1 to 3, and diffuse functions in both heavy atoms and hydrogens are necessary for proper treatment of hydrogen bonding (HB), we chose the aug-cc-pVTZ basis set as a fair compromise between size and reliability. In different studies on HB, DFT calculations with a flexible enough basis have been found well suited to obtain geometries and energies in hydrogen bonded structures.[24−26]

Equilibrium geometries were fully optimized using analytic gradients without symmetry constraints. The interaction energy at every structure was then corrected for basis set superposition error (BSSE) by using the Boys−Bernardi counterpoise scheme[27] and the zero-point-energy correction (ZPEC) was also included. Electron densities were then obtained in single-point calculations at the corresponding optimized structures. Geometries and electron densities were determined with the GAUSSIAN 03 package.[28] The localization and characterization of bond critical points of the electron density according to the atoms in molecules (AIM) theory[29,30] was accomplished with MORPHY.[31]

III. Results and Discussion

A. Geometries and Energies. Both experimental techniques[32−34] and quantum chemical computations[35−37] indicate that nitric acid has a planar C_s geometry in the gas phase. Two additional nonplanar stable geometries were also identified in this work at relative energies with respect to the planar global minimum of more than 75 kcal/mol. No experimental and theoretical data for these structures were found, but the analysis of vibrational frequencies reveals that they correspond to true minima. Transition states between conformation I and II or III (see Figure 1) were calculated, finding differences of energy between I and II or I and III around 30 kcal/mol, which suggests a high stability for these conformations. Due to this large energy difference, one may conjecture that these nonplanar structures have little atmospheric interest; hence we have addressed them as isolated conformers and forming only the complex $NO_3^-HNO_3$. Optimized geometries of isolated HNO_3 molecules and NO_3^- ion are drawn in Figure 1 and the geometrical parameters found at various levels of theory are gathered in Table 1. As expected, HF results for HNO_3 show larger deviations from experiment but B3LYP and MP2 yield similar results that deviate from experimental values[33] less than 0.01 Å and 1° for bond lengths and angles, respectively. In both cases, structures II and III show shorter $r(O_1N_1)$ lengths, a significant increase of $r(N_1O_2)$ and $r(N_1O_3)$, and much shorter distances between oxygens 2 and 3 (results not shown). According to the Lewis representation,

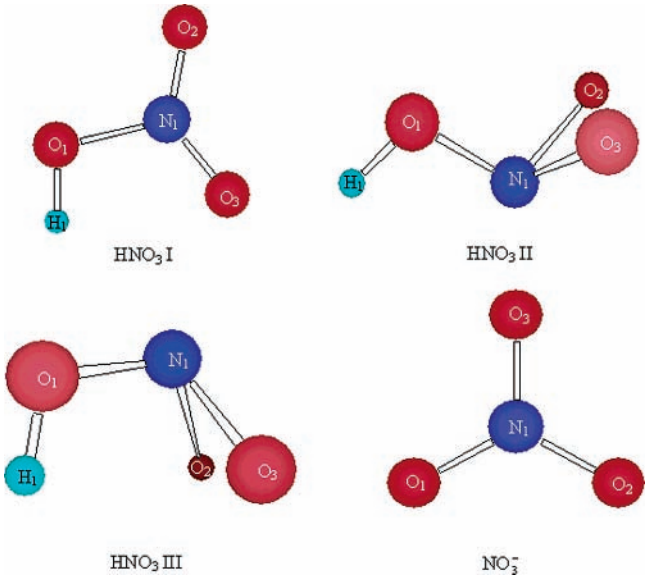

Figure 1. Equilibrium structures I−III for nitric acid and for nitrate ion.

TABLE 1: Equilibrium Geometries of Nitric Acid (Structures I−III) and Nitrate Displayed in Figure 1[a]

structures	parameters	HF[b]	B3LYP[b]	MP2[b]	exp[c]
HNO_3 I	$r(H_1O_1)$	0.956	0.972	0.973	0.964
	$r(O_1N_1)$	1.334	1.413	1.406	1.406
	$r(N_1O_2)$	1.173	1.192	1.202	1.199
	$r(N_1O_3)$	1.189	1.208	1.213	1.211
	$\theta(H_1O_1N_1)$	105.7	103.0	102.0	102.2
	$\theta(O_1N_1O_2)$	114.8	113.9	113.7	113.8
	$\theta(O_1N_1O_3)$	116.1	115.7	115.7	115.9
	$\tau(H_1O_1N_1O_2)$	180.0	180.0	179.9	180
	$\tau(H_1O_1N_1O_3)$	0.0	0.0	−0.1	0
HNO_3 II	$r(H_1O_1)$	0.951	0.967	0.969	
	$r(O_1N_1)$	1.347	1.388	1.386	
	$r(N_1O_2)$	1.354	1.411	1.420	
	$r(N_1O_3)$	1.354	1.411	1.420	
	$\theta(H_1O_1N_1)$	104.7	102.4	101.4	
	$\theta(O_1N_1O_2)$	108.4	107.5	106.7	
	$\theta(O_1N_1O_3)$	108.4	107.5	106.7	
	$\tau(H_1O_1N_1O_2)$	146.5	146.9	146.6	
	$\tau(H_1O_1N_1O_3)$	−146.5	−146.8	−146.8	
	ΔE	79.27	77.36	76.88	
HNO_3 III	$r(H_1O_1)$	0.958	0.976	0.977	
	$r(O_1N_1)$	1.334	1.361	1.359	
	$r(N_1O_2)$	1.362	1.426	1.438	
	$r(N_1O_3)$	1.362	1.426	1.438	
	$\theta(H_1O_1N_1)$	108.6	107.5	105.9	
	$\theta(O_1N_1O_2)$	110.4	109.9	108.9	
	$\theta(O_1N_1O_3)$	110.4	109.9	109.0	
	$\tau(H_1O_1N_1O_2)$	33.8	33.3	33.3	
	$\tau(H_1O_1N_1O_3)$	−33.8	−33.3	−33.3	
	ΔE	78.45	76.16	75.14	

structure	parameter	B3LYP[b]	MP2[b]	CCSD(T)[b]	MP2[d]
NO_3^-	$r(N_1O_1)$	1.258	1.261	1.261	1.2565
	$r(N_1O_2)$	1.258	1.261	1.261	1.2565
	$r(N_1O_3)$	1.258	1.261	1.261	1.2565
	$\theta(O_1N_1O_2)$	120.0	120.0	120.0	120.0
	$\theta(O_2N_1O_3)$	120.0	120.0	120.0	120.0
	$\tau(N_1O_1O_2O_3)$	180.0	180.0	180.0	180.0

[a] Bond lengths in Å; bond angles in degrees. ΔE (in kcal/mol) is the difference of energy (including zero-point correction for B3LYP and MP2) with respect to structure I. [b] aug-cc-pVTZ basis set, this work. [c] Reference 33. [d] MP2/aug-cc-pV5Z, ref 39.

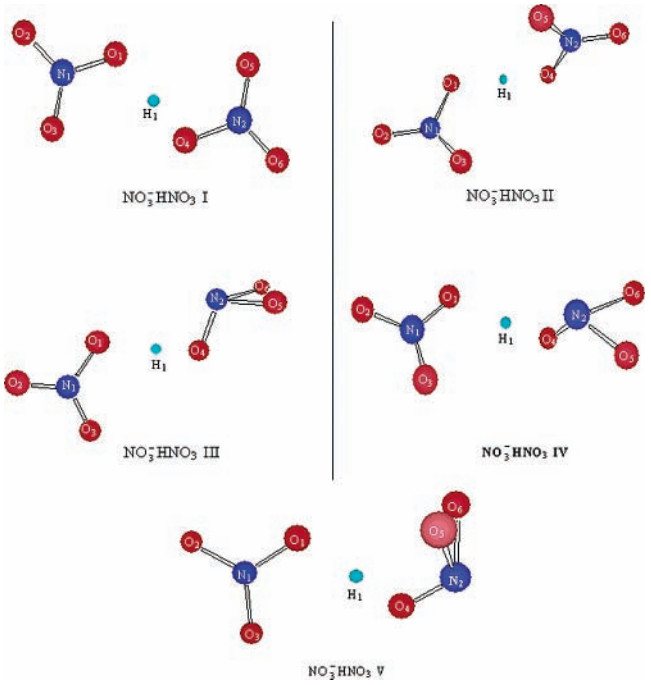

Figure 2. Equilibrium structures I−V for $NO_3^-HNO_3$.

structure I shows two "quasi-double" bonds for N_1O_2 and N_1O_3 (there are two resonance structures) and a larger single bond length for N_1O_1. The bond distances $r(N_1O_2)$ and $r(N_1O_3)$ are not equal because of the location of H_1. This situation changes for conformers II and III in which resonance structures are not possible, suggesting a different representation with a double bond for N_1O_1 and single bonds for N_1O_2 and N_1O_3. In agreement with the experimental observation,[38] our calculations yield for nitrate anion a D_{3h} structure with a bond length in good agreement with recent MP2 values reported by Wang et al.[39] B3LYP results are comparable to CCSD(T), which yields same values than MP2 method.

Figure 2 illustrates five equilibrium structures for the nitrate/nitric acid complex, also called hydrogen dinitrate ion. The first two aggregates are composed of structure I of nitric acid, complexes III and IV are formed with structure II, and the last one with structure III of nitric acid. Table 2 shows the geometrical parameters for the hydrogen bonds present in these complexes and the changes in relevant structural variables with respect to the monomers for the structures shown in Figure 2. Despite the different conformations of HNO_3, all the complexes show distances O···O ($r(O_4\cdots O_1)$ in Table 2) shorter than 2.60 Å for the $NO_3^-HNO_3$ complex, a value associated with strong HB in conventional classifications[40] (recall, for instance, that this O···O distance is about 2.9 Å in water dimer). The values of dissociation energies (D_0) in Table 2, similar to other SSHBs,[22] confirm the rather strong nature of hydrogen bonding in these systems. When we compare these distances with the B3LYP/aug-cc-pVTZ O···O length in nitric acid dimer, 2.745 Å, the negative charge of nitrate appears as the obvious responsible for such short hydrogen bond lengths. Similar D_0 and geometrical parameters (except for bond angle $\theta(O_1H_1O_4)$) are shown for the conformers I and II, which are composed of structure I of nitric acid. The dihedral angles between groups NO_3^- are the only noticeable geometrical difference between these conformers. Analogous features are found for conformers III and IV (composed of structure II of nitric acid). Conformation I has the lowest D_0 (−28.75 kcal/mol), the largest angle θ-$(O_1H_1O_4)$ (the closest to linearity), and a very short distance $r(O_1\cdots H_1)$. This C_s configuration is the structure of hydrogen dinitrate seen in tetraphenylarsonium salt.[17] However, $(O_2NO\cdot H\cdot ONO_2)^-$ appears in the crystalline state in rather distinct configurations, which differ in the relative orientation between the two O_2NO groups.[16,18] Structure II was predicted to be lower in energy than I by minimum-basis-set HF[20] and double-ζ plus polarization-on-heavy-atoms basis set Becke−Perdew density functional calculations;[21] however, our results predict a difference in energy between these structures of only about 0.06 kcal/mol for B3LYP and MP2 methods. This small difference indicates that there is a very low torsional barrier around the H-bond, which agrees with the wide range of structures found in the solid phase (ref 18 and references therein). Due to this fact, the dihedral angle between the two groups ONO_2^- varies from 180° (structure I) to 100° (structure II) for B3LYP and from 180° to 80° for MP2, but no minimum structures are found at angles close to 0°, a result that could be interpreted in terms of the high repulsion between oxygens 5 and 3 suggested by the structures shown in Figure 2. Due to conformation I being the global minimum, geometrical parameter will be described below in more detail. Conformations III and IV have higher D_0 (in absolute value) than V despite their longer H-bond lengths (see Table 2). This situation could be produced because of the shorter distances (around 3.3 Å for

TABLE 2: Equilibrium Geometries of H-Bonds and Changes of Intramolecular Parameters for $NO_3^-(HNO_3)_n$ ($n = 1-3$) Displayed in Figures 2 and 3[a]

$NO_3^-HNO_3$						$NO_3^-(HNO_3)_2$				$NO_3^-(HNO_3)_3$	
parameter	I	II	III	IV	V	parameter	HB-1	parameter	HB-2	parameter	HB-1
$r(H_1\cdots O_1)$	1.324	1.322	1.448	1.441	1.393	$r(H_1\cdots O_1)$	1.542	$r(H_2\cdots O_2)$	1.543	$r(H_1\cdots O_1)$	1.632
$r(H_1O_4)$	1.131	1.129	1.064	1.064	1.096	$r(H_1O_4)$	1.035	$r(H_2O_7)$	1.034	$r(H_1O_4)$	1.013
$r(O_4\cdots O_1)$	2.455	2.438	2.509	2.496	2.488	$r(O_4\cdots O_1)$	2.575	$r(O_7\cdots O_2)$	2.576	$r(O_4\cdots O_1)$	2.643
$\theta(O_1H_1O_4)$	179.1	167.9	174.6	170.0	177.7	$\theta(O_1H_1O_4)$	175.9	$\theta(O_2H_2O_7)$	177.8	$\theta(O_1H_1O_4)$	175.7
$\Delta r(N_1O_1)$	0.045	0.045	0.034	0.036	0.037	$\Delta r(N_1O_1)$	0.014			$\Delta r(N_1O_1)$	−0.005
$\Delta r(N_1O_2)$	−0.026	−0.026	−0.022	−0.022	−0.023	$\Delta r(N_1O_2)$	0.007				
$\Delta r(N_1O_3)$	−0.022	−0.023	−0.018	−0.019	−0.019	$\Delta r(N_1O_3)$	−0.031				
$\Delta\theta(O_2N_1O_3)$	3.4	3.4	2.7	2.7	2.8	$\Delta\theta(O_2N_1O_3)$	0.8			$\Delta\theta(O_2N_1O_3)$	0.0
$\Delta r(H_1O_4)$	0.159	0.157	0.097	0.097	0.120	$\Delta r(H_1O_4)$	0.063	$\Delta r(H_2O_7)$	0.062	$\Delta r(H_1O_4)$	0.041
$\Delta r(O_4N_2)$	−0.085	−0.085	−0.070	−0.071	−0.059	$\Delta r(O_4N_2)$	−0.058	$\Delta r(O_7N_3)$	−0.059	$\Delta r(O_4N_2)$	−0.048
$\Delta\theta(H_1O_4N_2)$	8.3	8.9	2.9	3.7	8.8	$\Delta\theta(H_1O_4N_2)$	5.8	$\Delta\theta(H_2O_7N_3)$	5.6	$\Delta\theta(H_1O_4N_2)$	4.7
$\Delta r(N_2O_5)$	0.016	0.015	0.040	0.032	0.050	$\Delta r(N_2O_5)$	0.008	$\Delta r(N_3O_8)$	0.008	$\Delta r(N_2O_5)$	0.006
$\Delta r(N_2O_6)$	0.031	0.031	0.039	0.067	0.051	$\Delta r(N_2O_6)$	0.022	$\Delta r(N_3O_9)$	0.021	$\Delta r(N_2O_6)$	0.017
D_0	−28.75	−28.69	−26.39	−26.35	−23.93	D_0	−46.04			D_0	−59.90

[a] Δr ($\Delta\theta$) is the difference of bond length (bond angle) between complexes and monomers. D_0 is the dissociation energy (including zero-point and BSSE correction) in kcal mol^{-1}. Bond lengths in Å, bond angles in degrees.

TABLE 3: Equilibrium Geometry I of $NO_3^-HNO_3$ Displayed in Figure 2[a]

parameter	B3LYP[b]	MP2[b]	TPA[c]
$r(N_1O_1)$	1.303	1.300	1.29
$r(N_1O_2)$	1.232	1.237	1.21
$r(N_1O_3)$	1.236	1.241	1.20
$r(O_4\cdots O_1)$	2.455	2.443	2.45
$r(H_1\cdots O_1)$	1.324	1.312	
$r(H_1O_4)$	1.131	1.131	
$r(N_2O_4)$	1.328	1.324	1.29
$r(N_2O_5)$	1.224	1.230	1.20
$r(N_2O_6)$	1.223	1.229	1.21
$\theta(O_1N_1O_2)$	117.7	117.8	119
$\theta(O_2N_1O_3)$	123.4	123.5	118
$\theta(O_4H_1O_1)$	179.1	179.2	180
$\theta(N_2O_4H_1)$	111.3	109.0	112
$\theta(O_4N_2O_5)$	118.8	118.6	119
$\theta(O_6N_2O_4)$	116.2	116.2	122
$\tau(O_4H_1O_1N_1)$	3.2	0.0	0

[a] Bond lengths in Å, bond angles in degrees, [b] aug-cc-pVTZ basis set, this work. [c] Reference 17. Distances and angles are the average between the equally probable alternative positions of oxygens for hydrogen dinitrate ion in tetraphenylasonium (TPA) hydrogen dinitrate.

TABLE 4: Equilibrium Geometries of the Most Stable Geometries of Complex $NO_3^-(HNO_3)_2$ and $NO_3^-(HNO_3)_3$ Displayed in Figure 3[a]

parameter	B3LYP	parameter	B3LYP
	$NO_3^-(HNO_3)_2$		
$r(N_1O_2)$	1.265	$r(N_3O_8)$	1.216
$r(N_1O_3)$	1.227	$r(N_3O_9)$	1.213
$r(N_1O_1)$	1.272	$\theta(O_2N_1O_3)$	120.8
$r(O_4\cdots O_1)$	2.575	$\theta(O_2N_1O_1)$	118.0
$r(H_1\cdots O_1)$	1.542	$\theta(O_4H_1O_1)$	175.9
$r(H_1O_4)$	1.035	$\theta(N_2O_4H_1)$	108.8
$r(N_2O_4)$	1.355	$\theta(O_4N_2O_5)$	118.2
$r(N_2O_5)$	1.216	$\theta(O_6N_2O_4)$	115.0
$r(N_2O_6)$	1.214	$\theta(O_2H_2O_7)$	177.8
$r(O_7\cdots O_2)$	2.576	$\theta(N_3O_7H_2)$	108.6
$r(H_2\cdots O_2)$	1.543	$\theta(O_8N_3O_7)$	118.2
$r(H_2O_7)$	1.034	$\theta(O_9N_3O_7)$	115.0
$r(N_3O_7)$	1.354		
	$NO_3^-(HNO_3)_3$		
$r(N_1O_1)$	1.253	$\theta(O_1N_1O_2)$	120.0
$r(O_4\cdots O_1)$	2.643	$\theta(O_2N_1O_3)$	120.0
$r(H_1\cdots O_2)$	1.632	$\theta(O_4H_1O_1)$	175.7
$r(H_1O_4)$	1.013	$\theta(N_2O_4H_1)$	107.7
$r(N_2O_4)$	1.365	$\theta(O_4N_2O_5)$	117.8
$r(N_2O_5)$	1.214	$\theta(O_6N_2O_4)$	114.7
$r(N_2O_6)$	1.209		

[a] Bond lengths in Å and bond angles in degrees.

conformation V and 4.3 Å for conformation III and IV) between the oxygens 5 and 6 of nitric acid and O_1 of nitrate, which could give rise to larger electrostatic repulsions. Our B3LYP and MP2 results for all these structures also show that the hydrogen atom remains bound to oxygen 4, which belongs to the nitric acid monomer, so that, in disagreement with the supposition made by experimentalists,[16−18] no C_2 symmetry axis is found.

Regarding the geometrical changes of the monomers when complexes are formed (see Table 2), $\Delta r(N_1O_1)$ has positive values for the five conformations, so this bond elongates upon complex formation, a feature found for conventional H-bonds.[41,42] This length increasing is compensated with shorter distances $r(N_1O_2)$ and $r(N_1O_3)$. Bond angles of nitrate do not undergo strong changes, increasing only about 2 or 3° for $\theta(O_2N_1O_3)$, which is offset by a slight decreasing in $\theta(O_1N_1O_2)$ and $\theta(O_1N_1O_3)$ (values not shown). The bond length difference $\Delta r(H_1O_4)$ undergoes the largest increasing with relative variations from 10 to 16% with respect to the monomer, a typical

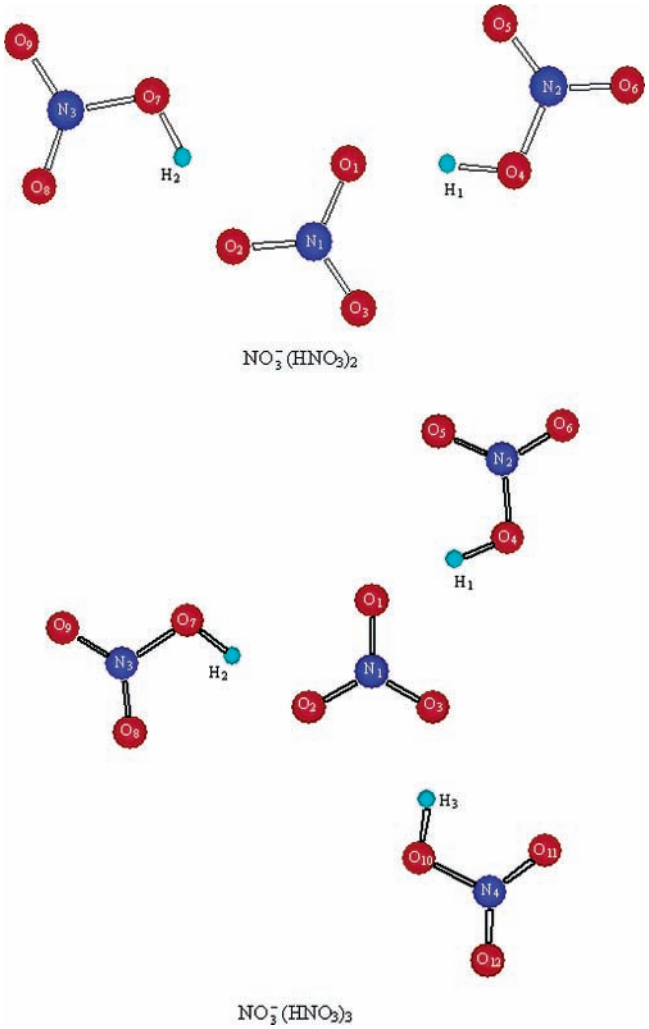

Figure 3. Equilibrium structures for $NO_3^-(HNO_3)_2$ and $NO_3^-(HNO_3)_3$.

feature of SSHBs too.[40] Also, longer distances $r(N_2O_5)$ and $r(N_2O_6)$, angle $\theta(H_1O_4N_2)$, and shorter $r(O_4N_2)$ are shown for the nitrate/nitric acid complexes. The last parameter tends to undergo a larger decrease for complexes with higher D_0. This feature agrees with the results found for conventional H-bonds, which show a larger decrease of the distance R−A (in a typical H-bond represented as: R−A-H···B−R′) for shorter H···B length.[43]

Table 3 shows geometrical parameters for the most stable equilibrium geometry of hydrogen dinitrate ion (structure I). Our B3LYP and MP2 results display similar values for all the parameters with differences smaller than 0.01 Å for bond lengths and 2° for bond angles. These results are compared with experimental values for the hydrogen dinitrate ion in tetraphenylarsonium salt, which has a structure similar to that of conformation I in Figure 2. All the NO bond lengths in this compound agree with our calculations for hydrogen dinitrate, with distances close to 1.3 Å for oxygens bonded to hydrogen and 1.2 Å for the rest. It must be also noted that the experimental $O_4\cdots O_1$ distance is rather similar to our calculated data, showing values about 2.45 Å indicative of a quite short H-bond.

Optimized geometries of $NO_3^-(HNO_3)_2$ and $NO_3^-(HNO_3)_3$ are displayed in Figure 3, and their geometrical parameters are collected in Table 4. Because B3LYP calculations require much less computational time than MP2 and, as demonstrated above, their results are comparable, we have considered only the B3LYP method to address these larger complexes. To the best

TABLE 5: Vibrational Frequencies (in cm^{-1}) at B3LYP and MP2 Level, Intensity Values (km/mol) at B3LYP Level, and Description in Terms of Internal Modes and Potential Energy Distribution (PED) for Nitrate Ion and Nitric Acid[a]

assignment, normal mode	approximate description (PED)[b]	B3LYP	MP2	intensity	exp
	NO_3^-				
asymmetric stretch NO_2 (2E′)	33 $r(N_1O_1)$ + 16 $r(N_1O_2)$ + 16 $r(N_1O_3)$ + 17 $\theta(O_2N_1O_3)$	1363	1472	572	1390[c]
symmetric stretch NO_2 (2E′)	33 $r(N_1O_2)$ + 33 $r(N_1O_3)$ + 17 $\theta(O_1N_1O_2)$ + 17 $\theta(O_1N_1O_3)$	1363	1472	572	1390[c]
stretch ip NO_3 (1A1′)	33 $r(N_1O_1)$ + 33 $r(N_1O_2)$ + 33 $r(N_1O_3)$	1061	1065	0	
bend oop NO_3 (1A2″)	100 τ ($N_1O_1O_2O_3$)	845	840	8	830[c]
symmetric bend NO_2 (1E′)	20 $\theta(O_1N_1O_2)$ + 20 $\theta(O_1N_1O_3)$ + 41 $\theta(O_2N_1O_3)$	707	713	0	720[c]
asymmetric bend NO_2 (1E′)	41 $\theta(O_1N_1O_2)$ + 41 $\theta(O_1N_1O_3)$	707	713	0	720[c]
	HNO_3 (C1)				
stretch O−H (A′)	93 $r(H_1O_1)$	3714	3718	94	3522[d]
asymmetric stretch NO_2 (A′)	27 $r(N_1O_2)$ + 23 $r(N_1O_3)$ + 24 $\theta(H_1O_1N_1)$ + 13 $\theta(O_1N_1O_3)$ + 11 $\theta(O_1N_1O_2)$	1744	1846	413	1699[d]
symmetric stretch NO_2 (A′)	32 $\theta(H_1O_1N_1)$ + 20 $r(N_1O_2)$ + 14 $r(N_1O_1)$ + 12 $r(N_1O_3)$	1342	1344	302	1321[d]
bend NOH (A′)	42 $\theta(H_1O_1N_1)$ + 24 $r(N_1O_3)$	1317	1315	52	1304[d]
stretch N−O (A′)	35 $r(N_1O_1)$ + 27 $\theta(O_2N_1O_3)$ + 14 $\theta(O_1N_1O_3)$ + 13 $\theta(O_1N_1O_2)$	896	894	183	897[d]
bend oop ONO_2 (A″)	59 τ ($H_1N_1O_1O_3$) + 41 τ ($H_1N_1O_1O_2$)	785	774	10	764[d]
bend scissor NO_2 (A′)	43 $r(N_1O_1)$ + 20 $\theta(O_2N_1O_3)$ + 14 $\theta(O_1N_1O_2)$	648	665	18	656[d]
bend ip ONO_2 (A′)	34 $\theta(O_1N_1O_3)$ + 34 $\theta(O_1N_1O_2)$ + 20 $\theta(H_1O_1N_1)$	585	589	6	588[d]
torsion H−ONO_2 (A″)	51 τ ($H_1O_1N_1O_2$) + 49 τ ($H_1O_1N_1O_3$)	491	485	115	451[d]

[a] The symmetry label of the internal mode according to the point group of the molecule is indicated in parentheses. [b] PEDs elements lower than 10% are not included. [c] Reference 45. [d] Reference 46.

of our knowledge, these are the first structures reported for these molecular systems. It is important to highlight that no optimized geometries were found to display hydrogen bonding between nitric acid molecules for the complex $NO_3^-(HNO_3)_2$. When a second nitric acid is added to hydrogen dinitrate ion, this molecule happens to be bound to nitrate instead of nitric acid. Even if we start the optimization process with an initial configuration of the type $(NO_3\cdots HNO_3\cdots HNO_3)^-$, a proton transfer between nitrate and HNO_3 bonded to it occurs upon relaxing the system, obtaining again the structure shown in Table 4. This fact highlights the great tendency toward aggregation between nitrate ion and nitric acid molecule. Although small deviations from planarity are found in these geometries, given the accuracy of our calculations and the convergence criteria chosen in the optimizations, we can consider that $NO_3^-(HNO_3)_2$ and $NO_3^-(HNO_3)_3$ have planar structures. $NO_3^-(HNO_3)_2$ shows C_s symmetry with similar geometrical parameters for the two H-bonds, and only small differences between O−H···O angles. $NO_3^-(HNO_3)_3$ has C_{3h} symmetry and hence the three H-bonds exhibit identical values and same internal variables as nitric acid (because of this symmetry, Table 4 lists only geometry data for one of the H-bonds). Distances O···H increase with the number of HNO_3 attached to the central NO_3^-, which presumably indicates weaker H-bonds formed. If we consider both H-bonds in $NO_3^-(HNO_3)_2$ equivalent, the dissociation energies per HB for complexes $NO_3^-(HNO_3)_n$ are −28.75 (conformation I), −23.02 and −19.97 kcal/mol for $n = 1-3$, respectively. A larger difference is obtained for the addition of a second molecule of nitric acid to the complex than for the transition between two and three HNO_3 molecules. Previous studies within the AIM theory[29,30] have emphasized the relationship between H-bond length and electron density values at bond critical points, ρ_C, with longer bonds showing smaller values of ρ_C.[41,44] For complexes $NO_3^-(HNO_3)_n$ $n = 1-3$, the ρ_C values at the corresponding H-bond paths are 0.127, 0.070, and 0.056 au, respectively. These values suggest that weaker H-bonds are formed for the addition of more HNO_3 and this weakening is larger for the transition between one and two molecules. Also, the linearity of the HB (angle ($O_4H_1O_1$)) decreases from $n = 1-3$. Table 2 shows that for $NO_3^-(HNO_3)_2$, N_1O_1 and N_1O_2 distances increase (in both cases the oxygen is the acceptor of an H-bond) when the complex is formed. This length increasing is compensated by a shorter distance for N_1O_3 bond, which does not participate directly in the formation of the HB. As indicated above, this feature was also found for $NO_3^-HNO_3$ with larger variations due to the greater strength of the H-bond. For both complexes, ρ_C at N−O bond paths involved in the formation of H-bonds decreases (0.049 au for N_1O_1 in $NO_3^-HNO_3$ and around 0.010 au for N_1O_1 and N_1O_2 in $NO_3^-(HNO_3)_2$), and increases for the rest of N−O bond paths of nitrate (around 0.030 au for N_1O_2 and N_1O_3 in $NO_3^-HNO_3$ and 0.040 au for N_1O_3 in $NO_3^-(HNO_3)_2$). However, all these distances decrease (see Table 2) and their ρ_C increase (around 0.008 au for all the N−O bond paths of nitrate ion) for $NO_3^-(HNO_3)_3$, contrary to the results described above for the others complexes. If we did not make any distinction among the three N−O bonds of nitrate, total variations of these distances (i.e., $\Delta r(N_1O_1) + \Delta r(N_1O_2) + \Delta r(N_1O_3)$) for complexes $NO_3^-(HNO_3)_n$ are −0.003, −0.010 and −0.015 Å for $n = 1-3$, respectively, which corresponds with total increases of ρ_C of 0.011, 0.018 and 0.023 au. These results suggest the existence of cooperative effects for the addition of HNO_3 molecules to the central NO_3^- ion responsible for this increase in the electron density at the B−R′ bond path. For both complexes, the variations in the rest of intramolecular geometrical parameters have the same behavior as the hydrogen dinitrate ion commented before; only the magnitude of these variations decreases from $n = 1$ to 3.

B. Frequencies. In the present work we have carried out B3LYP calculations of the vibrational spectra for the global minimum geometries of the monomers and the aggregates formed by nitrate ion plus up to three units of nitric acid. To help in possible future assignments of experimental spectra, infrared intensities (in addition to vibrational frequencies) are included in Tables 5−7, although only frequencies are discussed in the present paper. For the sake of comparison, frequencies of monomers have also been calculated at the MP2 level of theory with the same basis set used with the DFT method. These results along with the available experimental ones are collected in Table 5. It is clear from this table that MP2 generally overestimates frequencies, leading to differences with the experimental values lower than 6% in nitrate and close to 9% in nitric acid. These values would yield a closer agreement with the experimental results in the case that anharmonic corrections were taken into account. In turn, B3LYP calculations tend to underestimate frequencies in the case of nitrate ion (less than 2%) but produce values similar to those of MP2 for the nitric

TABLE 6: Vibrational Frequencies (in cm^{-1}), Intensity Values (km/mol), and Description in Terms of Internal Modes and Potential Energy Distribution (PED) for the Hydrogen Dinitrate Ion

assignment, normal mode	approximate description (PED)[b]	B3LYP	intensity	exp
bend NOH (A′)	15 $\theta(H_1O_4N_2)$ + 14 $r(O_4H_1)$ + 12 $r(O_1H_1)$ + 12 $\theta(N_1O_1H_1)$	1765	772	1688[c]
asymmetric stretch NO_2 (HNO_3) (A′)	15 $r(N_2O_6)$ + 12 $r(H_1O_4)$ + 12 $r(O_1H_1)$ + 10 $r(N_2O_5)$	1531	5	
stretch O−H + asymmetric stretch NO_2 (nitrate) (A′)	19 $r(H_1O_4)$ + 17 $r(O_1H_1)$	1506	216	
asymmetric stretch NO_2 (nitrate) (A′)	13 $r(N_1O_3)$ + 12 $r(N_1O_2)$	1471	910	1430[d]
global symmetric (symmetric stretch NO_2 (HNO_3) + symmetric stretch NO_2 (nitrate)) (A′)	12 $r(N_2O_4)$ + 12 $r(N_1O_1)$ + 11 $r(N_2O_5)$ + 10 $r(N_1O_3)$	1350	3	
torsion H−ONO_2 (A″)	100 τ(H)	1247	62	
stretch O−H + stretch ip NO_3 (A′)	25 $r(H_1O_4)$ + 15 $r(H_1O_1)$	1085	749	
stretch N−O (A′)	23 $r(N_2O_4)$ + 17 $r(H_1O_1)$	1023	36	
stretch O−H + symmetric stretch NO_2 (nitrate) (A′)	25 $r(H_1O_4)$ + 17 $r(H_1O_1)$ + 11 $r(N_1O_1)$	942	2193	
bend oop NO_3 (A″)	100 τ ($O_1N_1O_2O_3$)	833	9	797[c]
bend oop ONO_2 (A″)	100 τ ($O_4N_2O_5O_6$)	821	12	797[c]
asymmetric bend NO_2 + stretch O−H	25 $r(H_1O_1)$ + 14 $r(H_1O_4)$ + 11 $\theta(O_1N_1O_2)$	735	484	
symmetric bend NO_2 (A′)	19 $\theta(O_2N_1O_3)$ + 14 $\theta(O_1N_1O_3)$ + 10 $r(N_1O_1)$	717	1	
bend scissors NO_2 (A′)	17 $r(O_1H_1)$ + 16 $\theta(O_5N_2O_6)$ + 12 $r(H_1O_4)$ + 11 $\theta(O_4N_2O_5)$	697	151	
bend ip ONO_2 (A′)	29 $r(O_1H_1)$ + 25 $r(O_4H_1)$ + 10 $\theta(O_4N_2O_6)$	599	1221	
stretch O···O (A′)	41 $r(O_1H_1)$ + 22 $r(O_4H_1)$	239	859	
bend ip O−H···O (A′)	28 $r(O_1H_1)$ + 17 $\theta(N_1O_1H_1)$ + 15 $r(O_4H_1)$ + 11 $\theta(H_1O_4N_2)$	135	41	
bend oop O−H···O (A″)	49 τ ($O_1N_1O_2O_3$) + 48 τ ($O_4N_2O_5O_6$)	102	0	
aceptor wag (A′)	20 $\theta(N_1O_1H_1)$ + 14 $r(O_4H_1)$ + 20 $\theta(H_1O_4N_2)$	86	5	
Aceptor twist (A″)	36 τ ($O_1N_1O_2O_3$) + 29 τ ($O_4N_2O_5O_6$)	51	1	
torsion HB (A″)	50 τ ($N_1O_1O_4N_2$)	29	0	

[a] The symmetry label of the normal mode according to the point group of the molecule is indicated in parentheses. A dashed line indicates division between intra- and intermolecular normal modes. [b] PEDs elements lower than 10% are not included. [c] Reference 47. [d] Reference 18.

TABLE 7: Vibrational Frequencies (in cm^{-1}), Intensity Values (km/mol), and Description in Terms of Internal Modes[a]

Nitric Acid

	$NO_3^-(HNO_3)_2$				$NO_3^-(HNO_3)_3$	
	nitric acid 1[b]		nitric acid 2[b]			
assignment, normal mode	freq	int	freq	int	freq	int
stretch O−H (A′)	2630 (−1084)	1200	2558 (−1156)	4346	2988 (−726)	4
asymmetric stretch NO_2 (A′)	1684 (−60)	294	1685 (−59)	192	1692 (−52)	8
bend NOH (A′)	1505 (+188)	32	1485 (+168)	118	1458 (+141)	0
symmetric stretch NO_2 (A′)	1355 (+13)	8	1330 (−13)	357	1338 (−4)	0
torsion H−ONO_2 (A″)	1071 (+580)	81	1059 (+568)	52	977 (+486)	195
stretch N−O (A′)	978 (+82)	229	979 (+82)	71	963 (+67)	3
bend oop ONO_2 (A″)	809 (+24)	26	808 (+24)	0	804 (+19)	29
bend scissor NO_2 (A′)	698 (+51)	3	696 (+48)	18	694 (+46)	0
bend ip ONO_2 (A′)	648 (+63)	10	655 (+70)	3	648 (+63)	0

Nitrate Ion

	$NO_3^-(HNO_3)_2$		$NO_3^-(HNO_3)_3$	
assignment, normal mode	freq	int	freq	int
asymmetric stretch NO_2 (A′)	1270 (−93)	2298	1392 (+29)	527
symmetric stretch NO_2 (A′)	1444 (+80)	859	1392 (+28)	533
stretch ip NO_3 (A′)	1067 (+6)	25	1082 (+21)	0
stretch oop NO_3 (A″)	835 (−10)	8	834 (−11)	5
symmetric bend NO_2 (A′)	748 (+41)	126	749 (+42)	54
asymmetric bend NO_2 (A′)	736 (+29)	11	749 (+42)	53

Intermolecular

	$NO_3^-(HNO_3)_2$				$NO_3^-(HNO_3)_3$	
assignment, normal mode	freq	int	freq	int	freq	int
stretch O···O (A′)	270	29	206	140	269	0
bend ip O−H···O (A′)	100	1	122	9	77	0
bend oop O−H···O (A″)	105	0	96	1	90	2
aceptor wag (A′)	29	0	85	0	82	0
aceptor twist (A″)	54	0	43	1	22	0
torsion HB (A″)	18	0	20	0	12	0

[a] Numbers in parentheses indicate frequency shifts with respect to the monomer ($\Delta\nu = \nu_{complex} - \nu_{monomer}$). [a] Nitric acid 1 is formed by the atoms H1, O4, N2, O5 and O6; nitric acid 2 is formed by the atoms H2, O7, N3, O8 and O9.

acid. In light of the results in the monomers, it is possible to conclude that although MP2 displays a slightly more uniform behavior than B3LYP in these systems, the differences between the two methods are small (as in the case of the geometry

analysis), and the latter can be used with the expectation of a level of accuracy similar to one provided by MP2, while keeping computational effort to a more moderate level.

The dimer formed by nitrate anion and nitric acid is a notably complex system bearing a vibrational spectrum composed of 21 normal modes and much harder to analyze than those of the monomers. It is in these cases where, despite their inherent limitations in accuracy, quantum-chemical methods can be of appreciable help in understanding the vibrational spectra. We provide in Table 6 a B3LYP calculation of harmonic frequencies along with an assignment of the corresponding modes in an attempt to analyze future experimental spectra. The description of normal modes in terms of the used internal coordinates has been carried out with the help of a potential energy distribution (PED) analysis. Only contributions of internal coordinates larger than 10% are collected in the table. The numbering of atoms in Figure 2, symmetry labels, and for the case of stretching NO_2 modes, the monomer to which belongs the normal mode are also included, so ambiguities in assignment are avoided. Due to the strength of the H-bond implied in this dimer (≈29 kcal/mol), the monomers undergo significant changes in their structures and vibrational frequencies when they become a part of the dimer, and the correlation between these dimeric modes and the corresponding ones in the monomers becomes often troublesome. This can be viewed as a consequence of the "mixing" of internal coordinates belonging to both monomers that the strong interaction produces. As a consequence of this effect, movements of atoms forming the H-bond, $O_4-H_1\cdots O_1$ in Table 6, are involved in most of vibrational frequencies (see PED analysis). One of most notorious features found in the spectrum of this aggregate is that the O−H stretching mode is severely red-shifted with respect to its value in the nitric acid, so that it no longer has the highest frequency in the dimer. This comes as no surprise because, as it is well-known, the O−H stretch normally experiences a red shift as a consequence of the hydrogen bond,[48] but what is remarkable here is the large amount of $\Delta\nu = \nu_D\ \nu_M = -2208\ cm^{-1}$. The same hydrogen bond interaction causes also a typical blue shift of 448 and 756 cm^{-1} on the NOH bending and torsion $H-ONO_2$, respectively, the NOH bending therefore becoming the highest frequency mode. Besides these dramatic changes, other relevant features can be observed in the inspection of Table 6. It is found that the frequencies of the modes containing asymmetric stretch NO_2 in the complex fall between the values of the corresponding normal modes in both monomers (Table 5), suggesting that the structure of the NO_3 groups in the dimer is intermediate between those of nitrate ion and nitric acid, as confirmed by the geometric parameters found in the present study. Due to this fact, this normal mode is blue-shifted 143 cm^{-1} for nitrate and red-shifted 213 cm^{-1} for nitric acid. The effect of the interaction can also be traced back to relative IR intensities. Although these values are not displayed on Table 6, the calculated relative IR intensity found to correspond to this asymmetric NO_2 stretch in the dimer is roughly speaking half its value on the monomers (where it is the most intense mode in both cases). Some other minor shifts have been observed in other normal modes, for instance in-plane stretch NO_3 also undergoes a blue shift of 24 cm^{-1}, so both stretching modes of nitrate are blue-shifted, which agrees with the "total decrease" of N−O distance of nitrate in these complexes. Intramolecular bending out-of-plane normal modes in the complex also fall between the values of the corresponding normal modes in both monomers, and the rest of the bending normal modes undergo blue shift. The analysis of the low-frequency region of the spectrum that corresponds to the six intermolecular normal modes shows the highest vibrational frequency for the stretch O···O normal mode, contrary to more conventional H-bonds in which it is often for bending modes.[42] In Table 6, some experimental values of the infrared spectrum in the solid phase are also included for the sake of comparison. Despite the difficult task of corresponding these measurements with the calculated values, a good concordance is shown for all the frequencies assigned, leading to differences lower than 5%.

Table 7 shows B3LYP harmonic frequencies for the aggregates $NO_3^-(HNO_3)_2$ and $NO_3^-(HNO_3)_3$. For the sake of simplicity, the table shows all the frequencies of $NO_3^-(HNO_3)_2$ and only 15 normal modes of A symmetry out of the 51 frequencies corresponding to $NO_3^-(HNO_3)_3$. Because of the C_{3h} symmetry of the latter complex, most of its vibrational spectrum appears as formed by sets of three modes: two degenerated modes (E symmetry) and the one of A symmetry that correlate with the HNO_3 modes. Supporting information of the total IR spectra and the assignments in terms of normal modes and PED of these complexes is available on request to the authors. As we mentioned in the analysis of geometries, the two H-bonds formed in the complex $NO_3^-(HNO_3)_2$ differ slightly from each other, especially in the O−H···O angles, and consequently they show some differences in the frequencies that involve these atoms, mainly in the intermolecular normal modes. The normal modes assigned to the corresponding ones in isolated nitric acid undergo similar variations for the two complexes, with larger changes for $NO_3^-(HNO_3)_2$ due to the greater strength of the H-bonds formed. These normal modes show shifts similar to those of a conventional H-bond, with the largest changes occurring for the stretch O−H, bend NOH, and torsion $H-ONO_2$,[42] as the case of hydrogen dinitrate ion. Regarding the normal modes assigned to the nitrate, we observe blue shifts for all the modes except for the out-of-plane stretch NO_3. We shall not go into detail here in the analysis of the spectral region between 1685 and 1270 cm^{-1}, which corresponds roughly to the NO_2 symmetric and asymmetric stretches, because, due to the large mixing of modes the correlation with the monomeric modes loses part of its meaning. Concerning the tetramer $NO_3^-(HNO_3)_3$ it is found that stretching modes of NO_2 groups and in-plane NO_3 are blue-shifted for the complex, which is consistent with the decrease of the distance N−O. We can also observe that generally the frequencies assigned to nitrate monomer are shifted by a larger amount in $NO_3^-(HNO_3)_3$ than $NO_3^-(HNO_3)_2$, contrary to what is found for the frequencies assigned to the nitric acid, and suggesting the existence of cooperative effects in the addition of HNO_3 molecules, as it was indicated in our geometry study above. Concerning the analysis of the intermolecular frequencies, it shows lower frequency values when the number of HNO_3 units is increased, which could be related to the smaller strength of the H-bonds formed. According to Table 7, stretch O···O and acceptor wagging do not seem to follow this trend, but if we also consider the two E symmetry frequencies of the complex $NO_3^-(HNO_3)_3$ (which have values lower than those of A symmetry for both normal modes), the "average frequency values" of each normal mode are smaller than those in the complex $NO_3^-(HNO_3)_2$, so the trend is also globally followed for these modes too.

C. Thermochemistry. Enthalpies, entropies and Gibbs free energies of formation and reaction have been calculated for the species studied in this paper. Our B3LYP results are gathered in Table 8 where we have also included the available experimental data. Due to the discrepancies of about 15% among different experimental values (see NIST Chemistry WeBook[52]),

TABLE 8: Thermodynamic Data Calculated for the Reactions $NO_3^-(HNO_3)_{n-1} + HNO_3 \rightarrow NO_3^-(HNO_3)_n$ at Room Temperature and at 233 K[a]

$n-1$, n	$\Delta H°_{n-1,n}$		$\Delta S°_{n-1,n}$		$\Delta G°_{n-1,n}$	
	B3LYP	exp	B3LYP	exp	B3LYP	exp
0, 1	−28.9	-27 ± 3[b]	−28.6	−23.9[c]	−20.4	-19 ± 5[b]
1, 2	−17.3	-16.0 ± 0.8[d]	−30.3	-23 ± 2[e]	−8.21	-9.0 ± 0.3[d]
2, 3	−13.6	-13.9 ± 1[e]	−25.8	-27 ± 4[e]	−5.91	-5.9 ± 0.4[d]

$n-1$, n	$(\Delta H°_{233})_{n-1,n}$		$(\Delta S°_{233})_{n-1,n}$		$(\Delta G°_{233})_{n-1,n}$	
	B3LYP	exp	B3LYP	exp	B3LYP	exp
0, 1	−29.0		−29.2		−22.2	
1, 2	−17.4	−18.4[f]	−30.8	−25[f]	−10.2	−12.6[f]
2, 3	−13.8	−16.0[f]	−26.5	−25[f]	−7.61	−10.2[f]

$n-1$, n	$\Delta H°_f$		$S°$	
	B3LYP	exp	B3LYP	exp
HNO_3	−28.9	−32.1[g]	63.6	63.7[g]
NO_3^-	−72.7	-73.3 ± 0.3[c]	58.7	

[a] Data for isolated monomers are also included. Enthalpies and Gibbs energies in kcal/mol and entropies in cal/(mol K). [b] Temperature-dependent equilibrium ion/molecule reaction method in ref. 49. [c] Reference 49. [d] Temperature-dependent association ion/molecule reaction method in ref. 19. [e] High-pressure mass spectrometry method in ref. 19. [f] ΔG was determined by using K_{eq}. $\Delta H = \Delta G + T\Delta S$ assuming $\Delta S = 25$ cal/(mol K).[50] [g] Reference 51.

we compare our B3LYP results with the measured data, which shows a lower interval of error. Let us denote $(n-1, n)$ the reactions in which complexes composed of one nitrate anion and $(n-1)$ nitric acid molecules add up one further nitric acid molecule. For the two first reactions (0, 1) and (1, 2), our computed values are in excellent agreement with the experimental results, only S is slightly overestimated. For reaction (2, 3) the agreement is even better, being the calculated values being within the experimental uncertainty. We also include in Table 8 the values of these magnitudes at the stratospherically relevant temperature of 233 K. Our ΔH^0_{233} calculated is in good agreement with the experimental values, especially for the reaction (1, 2). The values of ΔG^0_{233} reported in ref 50 were obtained assuming $\Delta S^0_{233} = 25$ cal/(mol·K) so, although they are not the result of a direct measurement, our calculations support such an assumption. Our computed enthalpies of formation and absolute entropies for isolated HNO_3 are also in excellent agreement with the values found in the literature. In the case of the ΔH^0_f for nitrate, our result of 73 kcal mol^{-1} corresponds rather well with the value 73.3 ± 0.3 kcal mol^{-1} given by Davidson et al.,[49] so that, considering the reliability shown by our computed data in all the cases studied here, this agreement lends support to the result by Davidson's group with respect to others.

Considering the dissociation energies shown in Table 2 as well as the ΔG^0_{233} for the $(n-1, n)$ reactions, we can understand the central role played by the NO_3^- in the stabilization of these aggregates. First of all, the nitrate ion has a closed-shell stable configuration that is responsible for its relatively long life in the stratosphere. The association of this ion with a relatively abundant neutral species as HNO_3 involves an important stabilization of the system, as shown by the high-energy dissociation values. The SSHB formed in these complexes seems the key issue to understand that process so this stabilization could explain that the simple aggregate $NO_3^-HNO_3$ was considered in the first studies as "*an ambient ion rather than a fragment*".[8] According to the relative energy calculated here for these complexes, $NO_3^-(HNO_3)_3$ is more stable than $NO_3^-(HNO_3)_2$, which in turn is more stable than $NO_3^-HNO_3$, but nevertheless, it is experimentally known that $NO_3^-(HNO_3)_2$ is the most abundant ion in a large range of altitudes.[12] We can observe in Table 8 that $-\Delta G_{233,(0,1)}$ are by far the largest values of the three possible aggregation reactions, the two other values also being negative but clearly smaller, particularly the formation of the tetramer has a value of $-\Delta G_{233,(2,3)} = 7.6$ kcal mol^{-1}according to our calculations. Obviously the reasons for the abundance of $NO_3^-(HNO_3)_2$ are difficult to be related exclusively with relative stability or Gibbs energy of the aggregation reaction of the various species studied here. Some other aspects including kinetic considerations should be taken into account to propose an explanation of this fact.

IV. Conclusions

We have studied the ion complexes $NO_3^-(HNO_3)_n$, $n = 1-3$, which are the most abundant negative ions in the low and middle stratosphere, by means of B3LYP/aug-cc-pVTZ ab initio calculations. Our main goal in exploring these systems is to elucidate their structure and vibrational spectrum for the first time, and also to gain insight into the nature of the short strong hydrogen bonds formed, which are responsible of their high stability and abundance.

Our structure and vibrational frequencies calculated for the monomers are in good agreement with the experimental values available. Also, B3LYP yields results similar to those provided by MP2 and CCSD(T) calculations for both monomers and $NO_3^-HNO_3$, showing the reliability of our method to address the larger complexes. For the nitric acid molecule, two additional conformations were identified at relative energies with respect to the global minimum of more than 75 kcal/mol. Due to this large energy difference, they are not likely to have important stratospheric implications and we focus only on the complexes formed with the global minimum geometries. The structure of the complexes was fully optimized and the interaction energy was calculated taking into account the BSSE and ZPE correction. Large values of D_0 were determined for all the complexes, confirming the formation of SSHB. The strongest interaction takes place for hydrogen dinitrate ion, giving rise to important changes in the global structure, especially the O−H bond, which is elongated around 15%. Although $NO_3^-HNO_3$ has a planar global minimum structure, a nonplanar conformation having virtually the same energy was found (energy-difference less than 0.1 kcal/mol). This fact could be the cause of the wide range of structures found in solid phase for this ion. Structures of $NO_3^-(HNO_3)_2$ and $NO_3^-(HNO_3)_3$ have been reported for the first time. Both complexes show planar geometries with the nitrate ion in a central position and HNO_3 molecules bonded to it, giving rise to a highly symmetric C_{3h} structure for $NO_3^-(HNO_3)_3$. No optimized geometries were found to display HB between nitric acid molecules for the complex $NO_3^-(HNO_3)_2$, highlighting the great tendency toward aggregation between nitrate ion and nitric acid molecule.

Harmonic frequencies were calculated for the global minimum structures of monomers and nitrate−nitric acid complexes. Due to the strong structural changes that the monomers undergo when the hydrogen dinitrate ion is formed, most of the normal modes are composed of a "mixing" of internal coordinates belonging to both monomers. Stretch O−H, bend NOH and torsion H−ONO_2 modes of the nitric acid are dramatically shifted upon complexes formation, as a consequence of the H-bonds. As an example to illustrate the magnitude of these shifts, the stretch O−H is red-shifted more than 2000 cm^{-1} in the formation of $NO_3^-HNO_3$ complex. The changes in these vibrational frequencies assigned to nitric acid monomer decrease

with the number of HNO_3 attached to the central NO_3^- as a consequence of weaker H-bonds formed. A contrary effect is shown by frequencies assigned to nitrate monomer, which are stronger shifted upon addition of nitric acid molecules, suggesting the existence of cooperative effects in the formation of such complexes.

Values of enthalpies, entropies, and Gibbs free energies of formation and reactions have been calculated for all the compounds studied. The results are in excellent agreement with the experimental values, being even within the experimental uncertainty for several cases. Because there is a great discrepancy among different measured values in the literature, the reliability shown by our results can help to assess the reliability of some of the experimental measurements. Our thermodynamic data are consistent with the experimental findings that reveal a large relative abundance of these complexes, although the major abundance of $NO_3^-(HNO_3)_2$ cannot be properly explained with the mere consideration of these data.

Acknowledgment. The authors gratefully acknowledge financial support from Dirección General de Investigación, Ministerio de Ciencia y Tecnología of Spain, Project BQU2002-04005.

References and Notes

(1) Aikin, A. C. *J. Geophys. Res.* **1997**, *102*, 12921.
(2) Castleman, A. W. Jr.; Tang I. N. *J. Chem. Phys.* **1972**, *57*, 3629.
(3) Arijs, E. *Planet. Space Sci.* **1992**, *40*, 255.
(4) D′Auria, R.; Turco, R. P. *Geophys. Res. Lett.* **2001**, *28*, 3871.
(5) Arnold, F.; Krankowsky, D.; Marien, K. H. *Nature* **1977**, 267.
(6) Beig, G.; Chakrabarty, D. K. *J. Atmos. Chem.* **1988**, *6*, 175.
(7) Fehsenfeld, F. C.; Howard, C. J.; Schmeltekopf, A. L. *J. Chem. Phys.* **1975**, *63*, 2835.
(8) Viggiano, A. A.; Arnold, F. *Planet. Space Sci.* **1981**, *29*, 895.
(9) Viggiano, A. A.; Schlager, H.; Arnold, F. *Planet. Space Sci.* **1983**, *31*, 813.
(10) Beig, G.; Walters, S.; Brasseur, G. *J. Geophys. Res.* **1993**, *98*, 12775.
(11) Arijs, E.; Nevejans, D.; Ingels, J.; Freserick, P. *Planet. Space Sci.* **1983**, *31*, 1459.
(12) Krieger, A.; Arnold, F. *Geophys. Res. Lett.* **1994**, *21*, 1259.
(13) Beig, G.; Brasseur, G. P. *J. Geophys. Res.* **2000**, *105*, 22671.
(14) Heitmann, H.; Arnold, F. *Nature* **1983**, *306*, 747.
(15) D′Auria, R.; Turco, R. P.; Houk K. N. *J. Phys. Chem. A* **2004**, *108*, 3756.
(16) Roziere, J.; Roziere-Bories, M. T.; Williams J. M. *Inorg. Chem.* **1976**, *15*, 2490.
(17) Faithful, B. D.; Wallwork, S. C. *J. Chem. Soc., Chem. Commun.* **1967**, 1211.
(18) Detoni, S.; Diop, L.; Gunde, R.; Hadži, D.; Orel, B.; Potier, A.; Potier, J. *Spectrochim. Acta* **1979**, *35A*, 443.
(19) Włodek, S.; Łuczyński, Z.; Wincel, H. *Int. J. Mass. Spectrom. Ion Phys.* **1980**, *35*, 39.
(20) Gunde, R.; Solmajer, T.; Azman, A.; Hadzi, D. *J. Mol. Struct.* **1975**, *24*, 405.
(21) Dunlap, B. I.; Doyle R. J., Jr. *J. Phys. Chem.* **1996**, *100*, 5281.
(22) Gómez, P. C.; Pacios, L. F. *Phys. Chem. Chem. Phys.* **2005**, *7*, 1374.
(23) Pacios, L. F.; Gálvez O.; Gómez, P. C. *J. Chem. Phys.* **2005**, *122*, 214307.
(24) Ozeryanskii, V. A.; Pozharskii, A. F.; Bienko, A. J.; Sawka-Dobrowolskaa, W.; Sobczyk, L. *J. Phys. Chem. A* **2005**, *109*, 1367.
(25) González, L.; Mó, O.; Yáñez, M.; Elguero, J.; *J. Chem. Phys.* **1998**, *109*, 2585.
(26) Rabuck, A. D.; Scuseria, G. E. *Theor. Chem. Acc.* **2000**, *104*, 439.
(27) Boys, S. F.; Bernardi, F. *Mol. Phys.* **1970**, *19*, 553.
(28) Frisch, M. J.; Trucks, G. W.; Schlegel, H. B.; Scuseria, G. E.; Robb, M. A.; Cheeseman, J. R.; Montgomery, J. A., Jr.; Vreven, T.; Kudin, K. N.; Burant, J. C.; Millam, J. M.; Iyengar, S. S.; Tomasi, J.; Barone, V.; Mennucci, B.; Cossi, M.; Scalmani, G.; Rega, N.; Petersson, G. A.; Nakatsuji, H.; Hada, M.; Ehara, M.; Toyota, K.; Fukuda, R.; Hasegawa, J.; Ishida, M.; Nakajima, T.; Honda, Y.; Kitao, O.; Nakai, H.; Klene, M.; Li, X.; Knox, J. E.; Hratchian, H. P.; Cross, J. B.; Adamo, C.; Jaramillo, J.; Gomperts, R.; Stratmann, R. E.; Yazyev, O.; Austin, A. J.; Cammi, R.; Pomelli, C.; Ochterski, J. W.; Ayala, P. Y.; Morokuma, K.; Voth, G. A.; Salvador, P.; Dannenberg, J. J.; Zakrzewski, V. G.; Dapprich, S.; Daniels, A. D.; Strain, M. C.; Farkas, O.; Malick, D. K.; Rabuck, A. D.; Raghavachari, K.; Foresman, J. B.; Ortiz, J. V.; Cui, Q.; Baboul, A. G.; Clifford, S.; Cioslowski, J.; Stefanov, B. B.; Liu, G.; Liashenko, A.; Piskorz, P.; Komaromi, I.; Martin, R. L.; Fox, D. J.; Keith, T.; Al-Laham, M. A.; Peng, C. Y.; Nanayakkara, A.; Challacombe, M.; Gill, P. M. W.; Johnson, B.; Chen, W.; Wong, M. W.; Gonzalez, C.; Pople, J. A., *GAUSSIAN 03*; Gaussian Inc.: Wallingford, CT, 2004.
(29) Bader, R. F. W. *Atoms in Molecules: A Quantum Theory*; Claderon, Oxford, U.K., 1990.
(30) Popelier, P. L. A. *Atoms in Molecules: An Introduction*; Prentice-Hall: Harlow, U.K., 2000.
(31) Popelier, P. L. A. *MORPHY 98*; UMIST: Manchester, U.K., 1998.
(32) Maxwell, L. R.; Mosley, V. M. *J. Chem. Phys.* **1940**, *8*, 738.
(33) Cox, A. P.; Riveros, J. M. *J. Chem. Phys.* **1965**, *42*, 3106.
(34) Ghosh, P. N.; Blom, C. E.; Bauer, A. *J. Mol. Spectrosc.* **1981**, *89*, 159.
(35) Jinshan, L.; Zhao, F.; Jing, F.; Xiao, H. *J. Mol. Struct. (THEOCHEM)* **2001**, *574*, 213.
(36) Drimitova, Y. *Spectrochim. Acta, Part A* **2004**, *60*, 1.
(37) Hart, J. R.; Thakkar, A. J. *J. Mol. Struct. (THEOCHEM)* **2005**, *714*, 217.
(38) Cotton, F. A.; Wilkinson, G. *Advances in Inorganic Chemistry*, 5th ed.; J. Wiley and Sons: New York, 2000; p 321.
(39) Wang, X. B.; Yang, X.; Wang, L. S.; Nicholas, J. B. *J. Chem. Phys.* **2002**, *116*, 561.
(40) Jeffrey, G. A. *An introduction to Hydrogen Bond*; Oxford University Press: Oxford, U.K., 1997.
(41) Gálvez, O.; Gómez, P. C.; Pacios, L. F. *J. Chem. Phys.* **2003**, *118*, 4878.
(42) Gálvez, O.; Gómez, P. C.; Pacios, L. F. *J. Chem. Phys.* **2001**, *115*, 11166.
(43) Gálvez, O. Estudio de la formación de dímeros con enlace de hidrógeno a través de la densidad electrónica, Universidad Complutense de Madrid, Madrid, 2002,
(44) Espinosa, E.; Molins, E.; Lecomte, C. *Chem. Phys. Lett.* **1998**, *285*, 170; Espinosa, E.; Lecomte, C.; Molins, E. *Chem. Phys. Lett.* **1999**, *300*, 745; Espinosa, E.; Alkorta, I.; Rozas, I.; Elguero, J.; Molins, E. *Chem. Phys. Lett.* **2001**, *336*, 457.
(45) Cotton F. A.; Wilkinson, G. *Chem. Phys. Lett.* **2001**, *336*, 485.
(46) Barnes, A. J.; Lasson, E.; Nielsen, C. J. *J. Mol. Struct.* **1994**, *322*, 165.
(47) Barliè, B.; Hadži, D.; Orel, B. *Spectochim. Acta* **1981**, *37A*, 1047.
(48) Fuster, F.; Silvi, B. *Theor. Chem. Acc.* **2000**, *104*, 13.
(49) Davidson, J. A.; Fehsenfeld, F. C.; Howard, C. J. *Int. J. Chem. Kinet.* **1997**, *9*, 17.
(50) Arnold, F.; Viggiano, A. A.; Schaler, H. *Nature* **1982**, *297*, 371.
(51) Chase, M. W. Jr., *NIST-JANAF Themochemical Tables*, 4th ed.; *J. Phys. Chem. Ref. Data, Monograph* **1998**, *9*, 1-1951.
(52) NIST Chemistry WebBook, http://webbook.nist.gov/chemistry/, released May 2005.